Spin-wave instability magnon distribution for parallel pumping in yttrium iron garnet films at 9.5 GHz

Pavel Kabos,* Michael Mendik,† Garrelt Wiese,‡ and Carl E. Patton
Department of Physics, Colorado State University, Fort Collins, Colorado 80523
(Received 18 September 1996)

Parallel-pumping spin-wave instability processes for 2-, 4.15-, and 6-μm-thick yttrium iron garnet films have been studied by microwave and Brillouin light-scattering techniques. The pump frequency was 9.5 GHz. The static and linearly polarized microwave fields were in plane. Butterfly curves of the instability threshold microwave-field amplitude vs the static field H were measured, along with companion determinations of the critical mode in-plane spin-wave polar-angle θ_k and in-plane wave-number k distributions vs H. The 4.15- and 6-μm-thick films show narrow distributions in the critical-mode θ_k values and broad distributions in the critical-mode k values which appear at threshold and extend to high power. For the 2-μm film, the critical-mode θ_k distribution is narrow just at the instability threshold. As the power is increased, the critical-mode θ_k distribution broadens and develops a bimodal character indicative of a splitting into two critical modes. These distributions also show considerable fine structure. The basic shape of the butterfly curve and the measured θ_k values for the 4.15- and 6-μm-thick films are in rough agreement with predictions from bulk theory, except that the measured k values are in the 10^4 rad/cm range rather than near zero. These measured k distributions are quite broad and also show significant structure. [S0163-1829(97)08217-9]

I. INTRODUCTION

An important precursor to the full understanding of nonlinear microwave phenomena in thin magnetic films is the identification of the spin-wave normal modes, called critical modes, which are excited when the applied microwave power exceeds the Suhl threshold for the generation of parametric spin waves. Several papers have reported on the direct experimental identification of these modes for parallel pumping,[1,2] subsidiary absorption,[3,4] and resonance saturation[5] configurations. Parallel pumping occurs with the linearly polarized microwave field parallel to the static magnetic field. Subsidiary absorption occurs when the microwave field is perpendicular to the static field. Both of these processes are connected with the parametric excitation of spin waves at one-half the pump frequency. For typical ferrite materials and a pump frequency ω_p in the 10 GHz range, these processes are allowed for a region of static field somewhat below the field required for ferromagnetic resonance (FMR). At high-power levels, one observes an additional region of high loss over this low-field range. The term ''subsidiary absorption'' refers to this additional loss at fields below FMR. Resonance saturation concerns the field region close to the FMR. At high power, the FMR response broadens and decreases due to the parametric excitation of spin waves at the pump frequency. Reference 5 provides a brief review of these effects and lists additional references.

The technique which was used in Refs. 1–5 to identify the relevant critical modes associated with the respective instability processes was Brillouin light scattering (BLS). The technique makes it possible to determine, within certain limits, both the magnitude and the direction of the spin-wave wave vector for the critical modes. In some instances, the BLS results provided a direct confirmation of the predictions from bulk theory for the critical modes. In others, the data provided an indication of new effects. For subsidiary absorption, the main new effect was a rather wide range of wave numbers for the critical modes above threshold. From theory, one would expect a single well-defined value of the wave number k. For resonance saturation, the new results were in the discovery of low-k modes with an in-plane propagation angle close to 90° relative to the in-plane static field, rather than the 0° propagation angle expected from bulk theory.[5] Overall, these results indicate that spin-wave instability processes in thin films (1) are strongly affected by the thin-film geometry and (2) involve a wide distribution of critical modes rather than a single lowest threshold critical mode as expected from existing theory.

In this work, the measurements of critical-mode wave-vector distributions described in Refs. 4 and 5 for subsidiary absorption and resonance saturation are extended to the parallel-pumping configuration. This process was first discovered by Schlörmann, Green, and Milano.[6,7] For this configuration, with the microwave magnetic field parallel to the static field, there is no coupling between the microwave field and the usual FMR response and, hence, no high-power effect in the FMR regime. There is still an effect at low field, similar to the subsidiary absorption response, in which a direct coupling between the microwave pump field and spin waves at one-half the pump frequency ω_p leads to a nonlinear response. As in subsidiary absorption, one finds a threshold microwave-power level above which there is an abrupt increase in the microwave loss due to the parametric excitation of spin waves at $\omega_p/2$.

The BLS techniques are applicable to the parallel-pumping configuration.[1,2] In this work, these techniques have been used to measure the magnitude and direction of the spin-wave wave vector for the critical modes for in-plane magnetized films in the parallel-pumping configuration. The measured magnon distributions have characteristics which are similar to those for subsidiary absorption, with the criti-

 © 1997 The American Physical Society

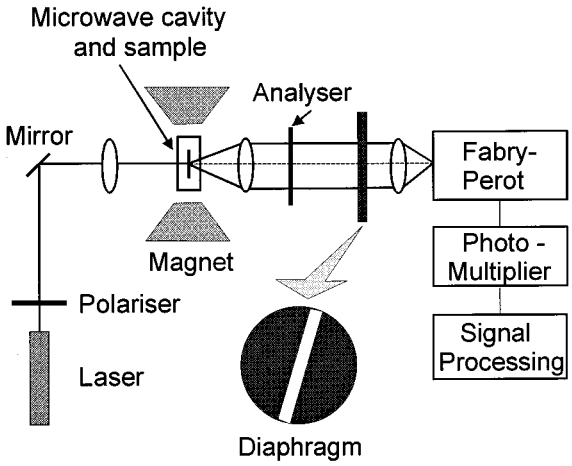

FIG. 1. Schematic diagram of the combined microwave parallel-pumping and forward Brillouin light-scattering experimental setup.

cal modes limited to relatively narrow-angle distributions, but with rather broad k distributions. In this work, several films of different thickness were examined. Significant differences were found between the thinnest 2-μm film and the two thicker 4.15- and 6-μm films.

II. EXPERIMENT

The combined microwave parallel-pumping and Brillouin light-scattering measurements were made with a standard reflection cavity arrangement in combination with a wave-vector and frequency-selective BLS setup.[1–5] The pump frequency was 9.5 GHz. The (111)-plane yttrium iron garnet (YIG) films were grown by liquid-phase epitaxy on gadolinium gallium garnet substrates at the Westinghouse Research and Development Center, Pittsburgh, PA. The measurements were made on films nominally 4 mm$\times$4 mm square and of three different thicknesses 2, 4.15, and 6 μm.

A schematic of the experimental system is shown in Fig. 1. The diagram shows the optical system for the forward-scattering BLS measurements, the microwave cavity for the microwave excitation, the magnet, the selective diaphragm in the collection optics, and the Fabry-Pérot, detection electronics, and signal-processing components. The diaphragm is critical to the wave-vector selection experiments and results to be considered below. The various system components are discussed below.

For microwave excitation, the YIG films were placed in the middle of a TE_{102} rectangular cavity, at the location of maximum microwave-field amplitude. The linearly polarized microwave field was parallel to the static external magnetic field H, with both fields in the plane of the film. Small openings in the front and rear wider sides of the rectangular cavity provided optical access to the sample. The loaded Q of the 9.5-GHz cavity was about 2000. The microwave power to the cavity was provided by a microwave sweep generator operating in a constant frequency mode. The cw microwave signal from the sweeper was amplified by a traveling-wave tube (TWT) amplifier. The microwave-power level, as measured at the TWT amplifier output, ranged from approximately 0.15 to 5 W. Threshold powers ranged from approximately 0.25 to 3 W, measured at this same point. Since the focus of this work is on magnon wave-vector distributions above threshold, no effort was made to calibrate the microwave system in terms of microwave-field amplitude vs incident power.

The BLS system was the same as described in Refs. 3 and 4. The combined BLS-microwave measurements were done in a forward-scattering configuration as shown in Fig. 1. The incident light is normally incident on the sample through one lens. The scattered light on the other side is collected and formed into a parallel beam by a second lens. There is also a small prism between the sample and the collection lens, not shown in Fig. 1, which is used for alignment purposes in a backscattering configuration. For wave-vector distribution measurements, a diaphragm with a 200-μm-wide slit extending across the whole diameter is placed after the collection lens. The axis and the orientation of this diaphragm then select the angle and wave number for the magnon, which gives rise to the scattered light to be analyzed. The scattered light is then directed to the input of a Sandercock-type high-contrast multipass tandem 3+3 Fabry-Pérot interferometer.[8] The intensity of the scattered light, at the frequency shifted by $\omega_p/2$ from the central Rayleigh peak in the BLS spectra, is then registered with the aid of the frequency-gating option of the Sandercock system. As discussed below, one may use the system to measure the scattered-light intensity as a function of several different control parameters such as the microwave power, magnon wave number k, wave vector angle, etc. The spin-wave instability effect is best observed from the dependence of the scattered-light intensity or photon count, as a function of microwave power at fixed H. The threshold is indicated by an abrupt rise in the light signal at some threshold power level P_{crit}. This determination is best made with the selective diaphragm removed from the optical path. The diaphragm is used for measurements at fixed-power levels above the threshold to determine magnon wave-number and angle distributions.

The collection optics arrangement determines the range of critical wave vectors that can be detected in the forward-scattering experiments. There are several limits which are important. First, the radius of the collection lens sets an upper limit on the magnitude of the in-plane wave-vector component which can be detected in the forward-scattering geometry. For the 488-nm-wavelength laser line and the 50-mm-focal-length and fl:1.4 collection lens used in this work, the upper limit on the in-plane wave-vector component amplitude which can be detected is about 4×10^4 rad/cm. Second, a small alignment prism between the sample and collection lens serves to block any scattered light which corresponds to very-low-angle scattering and very small magnon wave numbers. This blockage places a lower limit on the accessible wave-vector amplitudes of about 100 rad/cm or so.

Selection of the wave-vector propagation direction is accomplished with a rotatable and movable diaphragm plate behind the collection lens with a narrow 200-μm-wide slit. By rotating this diaphragm around the optical axis of the collection lens, one can select out the particular in-plane propagation direction of the excited spin waves. When the slit is aligned with the orientation of the in-plane static magnetic field H, one selects an in-plane wave vector with a polar angle of 0°. When the slit is rotated by 90°, the selected

polar angle is changed to 90°. In the actual experiment, the diaphragm is slowly rotated and the intensity of the scattered light passing through the slitted diaphragm is collected for a gated portion of the Fabry-Pérot free spectral range which corresponds to a spin-wave frequency $\omega_k = \omega_p/2$. The result is a direct measurement of the light-scattering intensity vs the polar spin-wave angle for critical modes with in-plane wave vectors in the range given above. As will be demonstrated shortly, one generally obtains critical modes with a narrow, well-defined polar spin-wave propagation angle θ_k. Once this critical-mode angle has been determined, rotation of the same slit diaphragm, with the axis shifted off of the optical axis, allows for the measurement of the scattering as a function of the amplitude of the in-plane wave vector or wave number k. No special attempt was made to check the sensitivity of the system with respect to the angle of rotation. Further details on the forward-scattering frequency and wave-vector-selective BLS technique can be found in the references cited above.

The abrupt increase in the scattered-light intensity which takes place in subsidiary absorption and parallel-pumping experiments as the microwave-field amplitude exceeds the spin-wave instability threshold and the critical modes are parametrically excited is described in detail in Refs. 1–5. Figure 3 of Ref. 5 shows a typical response and this result will not be repeated here. The basic result is that the BLS signal from excitations at $\omega_k = \omega_p/2$ remains at background levels until the microwave-field amplitude reaches the spin-wave instability threshold in power, P_{crit}, or the corresponding threshold in microwave-field amplitude at the sample position, h_{crit}. As the microwave power P and field h exceed this threshold, the intensity of the scattered light increases rapidly. The experiments cited above were the first to show direct correlations between the increase in the microwave loss above threshold and the parametric excitation of $\omega_p/2$ spin waves in thin films.

The threshold h_{crit} as a function of the static field H yields the same type of butterfly curve results as obtained previously by microwave techniques alone, but with additional information on the frequencies and wave vectors of the critical modes. The basic butterfly curve measurement for parallel-pumping and subsidiary absorption is described in Refs. 1–4. Here it will prove convenient to display butterfly curve data in a purely experimental way by plotting the square root of the ratio of the critical-power threshold P_{crit} to the minimum such critical power, $P_{\text{crit-min}}$, as a function of the static applied magnetic field H. Such a format avoids the problem of the microwave-pump-field calibration and still provides an overall picture of the butterfly-curve characteristics. In this study, one key result concerns the effect of film thickness on the butterfly-curve response. The normalized data format will demonstrate these effects uncluttered by problems of calibration. These curves of the threshold parameter $(P_{\text{crit}}/P_{\text{crit-min}})^{1/2}$ vs the static magnetic field H correspond to normalized butterfly curves of h_{crit} versus H.

The butterfly-curve data to be shown below were obtained with no diaphragm in place, in order to optimize the scattering signal. One has to keep in mind that for thresholds determined with no diaphragm, all the accessible critical modes contribute to the scattering. The light-scattering-determined butterfly curve is also limited to the high-field portion from

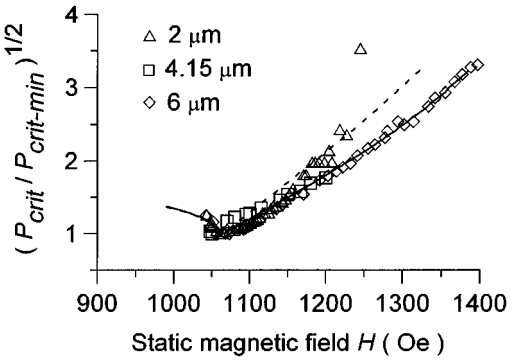

FIG. 2. Normalized parallel-pump butterfly curves of the spin-wave instability threshold microwave-field amplitude, expressed as the square root of the ratio of the threshold power at a given field P_{crit} to the minimum threshold power $P_{\text{crit-min}}$, as a function of the in-plane static magnetic field H. The pump frequency was 9.5 GHz. The open diamonds, open squares, and open triangles show the data for the 6-, 4.15-, and 2-μm-thick films, respectively. No wave-vector-selective diaphragm was used. Thresholds were determined from the increase of the BLS signal intensity corresponding to magnons at one-half the pump frequency. The solid and dashed lines show theoretical curves as discussed in the text.

near the minimum to the high-field $\omega_p/2$ spin-wave cutoff, rather than the entire range which is sampled by microwave techniques. The reason for this is that the range of critical-mode wave numbers which can be detected in the forward-scattering arrangement is limited to values below about 4×10^4 rad/cm. Once these threshold data were obtained, the diaphragm rotation schemes described above were used to obtain additional information on the wave-vector distributions for the critical modes above the threshold.

III. RESULTS

The normalized butterfly curves as measured for all three film samples are shown in Fig. 2. The open diamonds show the data for the 6-μm-thick film, the open squares show the data for the 4.15-μm-thick film, and the open triangles show the data for the 2-μm-thick film. The solid and dashed lines represent the results of calculations based on the bulk theory of Schlömann.[6,7] These curves will be discussed in the next section. For purposes of discussion, the results shown in Fig. 2 can be separated into three field regions, (i) fields below $H = 1040$ Oe where the data stop, (ii) fields between 1040 Oe and about 1150 Oe where the data for the three samples overlap, and (iii) fields above 1150 Oe where the data for the 2-μm-thick film fall above the data for the other two samples.

Consider region (i). For values of the static field below 1040 Oe, no light-scattering signal could be associated with a spin-wave instability at any power level up to the highest power available. This is a direct consequence of the limitation on detectable wave numbers in the BLS experiment as already mentioned. For field values below 1040 Oe, the expected critical modes have wave numbers greater than the maximum observable value of 4×10^4 rad/cm. Such high-k modes are not observed in the forward-scattering BLS experiment. This abrupt truncation in the BLS critical-mode signal provides a useful check on the experiment. If the in-

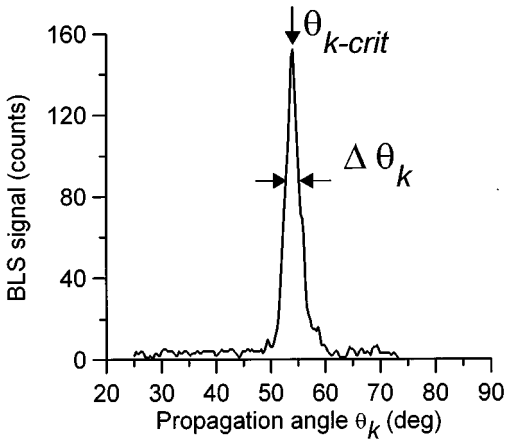

FIG. 3. Representative data on the BLS signal intensity as a function of the in-plane propagation angle θ_k. These data are for the 2-μm-thick-film, a static field of 1111 Oe, and a power level approximately 0.3 dB above threshold. The pump frequency was 9.5 GHz. As in Fig. 1, only the portion of the BLS signal corresponding to magnons at one-half the pump frequency was monitored. The arrow at the peak indicates the critical-mode central spin-wave propagation angle $\theta_{k\text{-crit}}$. The width at half height is indicated as $\Delta\theta_k$.

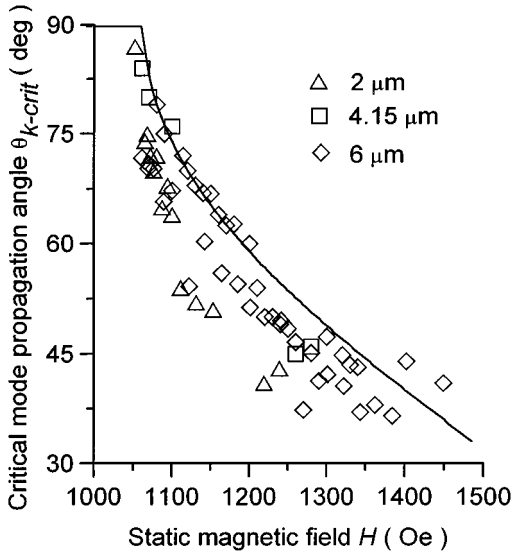

FIG. 4. Critical-mode in-plane propagation angle $\theta_{k\text{-crit}}$ vs the in-plane static magnetic field H, based on measurements of the type shown in Fig. 2 as a function of static field. The pump frequency was 9.5 GHz. The open diamonds, open squares, and open triangles show the data for the 6-, 4.15-, and 2-μm-thick films, respectively. The solid line shows the predicted result from bulk parallel-pumping spin-wave instability theory.

crease in the BLS signal were due to effects other than the parametric excitation of critical spin-wave modes, there would be no truncation.

In region (ii), for fields between 1040 and 1150 Oe, the normalized thresholds are about the same for all three films. It is to be noted that the actual thresholds in power as well as these normalized thresholds also matched in region (ii). This match-up could be taken to imply that the critical modes for these films are also similar for these films of different thicknesses in this field range. As will be discussed shortly, the critical modes for the thinnest film are quite different from those for the two thicker films. It is noteworthy that no differences are evident from the butterfly curve over this region of field.

In region (iii), for static fields above 1150 Oe, the normalized butterfly curve for the 2-μm-thick sample increases more rapidly than for the other films. This is the first indication, as far as the butterfly-curve data are concerned, that the details of the instability process might be affected by the film thickness.

Recall that the above measurements were obtained with no wave-vector-selective diaphragm in place. Measurements of the critical-mode in-plane propagation direction $\theta_{k\text{-crit}}$ were obtained for various fields and power levels above threshold by means of the rotatable slit diaphragm procedure described above. Some representative results are shown in Fig. 3. As before, only the BLS signal for $\omega_p/2$ magnons was monitored. For these θ_k determinations, the diaphragm was centered on the forward-scattering optical axis just behind the collection lens and slowly rotated. The BLS signal was recorded as a function of the rotation angle relative to the direction of the static field **H**. Recall that θ_k corresponds to the angle between the in-plane field direction and the in-plane component of the spin-wave wave vector **k**. If one takes the critical mode wave vector to be in plane, θ_k corresponds to the usual spin-wave wave-vector polar angle as well as the rotation angle in the experiment.

The particular data in Fig. 3 are for the 2-μm-thick film, a static field of 1111 Oe, and a power level of about 0.3 dB above threshold. The data show a sharp peak at an angle close to $\theta_k = 53°$, as indicated by an arrow and labeled as $\theta_{k\text{-crit}}$. The width at half maximum of the response is about 3°–4°. This half-width for the critical mode propagation angle distribution will be denoted as $\Delta\theta_k$. The peak position is somewhat smaller than the value of 72° predicted from bulk parallel-pumping theory. The narrow width indicates that the critical modes are well localized in terms of propagation angle for power levels which are just above threshold. As will be seen shortly, both the position and width of this critical mode θ_k response provide new information on the spin-wave instability processes for parallel pumping in thin films.

Measurements similar to those shown in Fig. 3 were obtained as a function of the static field H and the power level above threshold for all three films. Subtle but possibly significant differences were found for the variation in $\theta_{k\text{-crit}}$ with field and for the variation in $\Delta\theta_k$ with power for the thinnest 2-μm film, relative to the two thicker films. Results on the critical mode $\theta_{k\text{-crit}}$ variation with field H are shown in Fig. 4. These data were obtained for power levels a few tenths of a dB above threshold for a given field and are taken to represent the critical-mode spin-wave propagation angle just at threshold. The coding for the different films is the same as in Fig. 2, with open diamonds for the 6-μm film, open squares for the 4.15-μm film, and open triangles for the 2-μm film data. The solid line shows the predicted $\theta_{k\text{-crit}}$ versus H for the critical modes expected from the bulk theory.[6,7]

The results in Fig. 4 show that the experimentally determined critical-mode propagation angle follows the bulk-

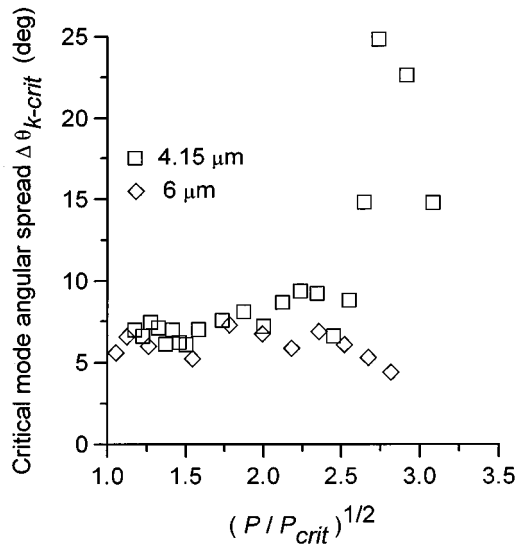

FIG. 5. Critical-mode propagation-angle half-width $\Delta\theta_k$ as a function of the normalized microwave-field amplitude parameter $(P/P_{\text{crit}})^{1/2}$. The open diamonds show the results for the 6-μm-thick film and a static magnetic field of 1100 Oe. The open squares show the results for the 4.15-μm-thick film and a field of 1070 Oe. The pumping frequency was 9.5 GHz.

theory prediction reasonably well. In spite of the large scatter in the data, the dropoff in the measured $\theta_{k\text{-crit}}$ with increasing field is somewhat more rapid than expected from the bulk theory and the most rapid falloff in $\theta_{k\text{-crit}}$ occurs for the thinnest film. The data in Fig. 4 do not show the same distinct separation in $\theta_{k\text{-crit}}$ versus field for the thinnest film, which is evident from the P_{crit} results in Fig. 2. The trend, nevertheless, is the same. There appears to be a difference in the behavior of the critical modes, even just at the threshold, for the thinnest film.

Measurements of critical-mode angle properties well above threshold also indicate significant differences as a function of film thickness. As an example, Fig. 5 gives the results of measurements of the width $\Delta\theta_k$ of the θ_k distribution as a function of $(P/P_{\text{crit}})^{1/2}$ for the two thicker films. The 6- and 4.15-μm data are indicated by the open diamond and open square symbols, respectively. The H values and corresponding $\theta_{k\text{-crit}}$ positions were not quite the same for the two sets of measurements. For the 6-μm-thick film, H and $\theta_{k\text{-crit}}$ were 1100 Oe and 67°, respectively. For the 4.15-μm-thick film, these values were 1070 Oe and 80°. These measurements were possible for the two thicker films because the $\theta_{k\text{-crit}}$ values for a given field did not change with power. Nevertheless, thickness effects are in clear evidence. The critical mode $\Delta\theta_k$ for the 6-μm-thick sample does not change significantly with $(P/P_{\text{crit}})^{1/2}$. The situation is different for the 4.15-μm film. Here one finds that $\Delta\theta_k$ increases significantly at the highest-power levels available. This result is particularly interesting because the two films have essentially the same critical-mode behavior just at threshold. No data are shown in Fig. 5 for the thinnest film 2-μm film. This is because the measurements of the BLS signal versus rotation angle for this sample at high-power levels did not yield single peaks with well-resolved θ_k values. It was not possible to define either $\theta_{k\text{-crit}}$ or $\Delta\theta_k$ in this case. The increase in $\Delta\theta_k$ with power for the 4.15 μm may be considered as a precursor to the more complicated θ_k response for the 2-μm film. Results for the 2-μm film will be considered in detail at the end of this section.

The conclusion from the above results is that the physics of the critical mode behavior for the parallel-pumping process, at threshold and above threshold as well, is *thickness* or in general size dependent. Size effects have been observed and partially explained for subsidiary absorption.[9] They may also be critical to the quantitative understanding of parallel pumping in thin films. These considerations will be discussed further below.

The considerations so far have concerned the instability thresholds and the propagation-angle characteristics for the critical modes. Now the wave-number distributions will be addressed. Recall that the above θ_k results were obtained with a combined microwave-BLS spectrometer with a slitted diaphragm positioned behind the collection lens and aligned along the optical axis. The angle data were obtained by rotating the diaphragm. The slit in the diaphragm is narrow, but extends over the whole diameter of the collection lens. In this configuration, the diaphragm selects the angle, but not the wave number. That is, all the spin waves which propagate in the selected direction defined by the slit orientation contribute to the scattered-light intensity over the entire range of wave numbers accessed by the lens.

The fact that the angle distributions for the critical modes are reasonably narrow for the two thickest films makes it possible to use the same slit diaphragm arrangement to obtain wave-number distributions for the critical modes, as well. This is accomplished by simply shifting the axis of the diaphragm off the optical axis before rotation. Rotation of the shifted diaphragm causes the slit to intersect the slice of wave vectors at a given θ_k value at different distances from the optical axis. This intersection corresponds to specific in-plane components of the critical-mode wave vector. Data collection as a function of a rotation angle then yields results on the wave-number distribution for the critical mode at the selected value of θ_k.

Some results from combined propagation-angle and wave-number distribution measurements are shown in Fig. 6. The data shown are for the 4.15-μm-thick film at two power levels 2 and 6 dB above threshold. The two left-hand-side diagrams in Fig. 6 show the measured BLS signal versus rotation for a static magnetic field of 1070 Oe. These data are similar to the data in Fig. 3 except that the power levels are now well above threshold. These data show that the angle distributions do not change significantly with power above threshold. The peak in the BLS signal occurs at $\theta_{k\text{-crit}} \approx 80°$, independent of the power. The right-hand-side diagrams in Fig. 6 show the results of the measurements with the diaphragm axis off the optical axis. For these diagrams, the rotation has been converted to a scale for the in-plane spin-wave wave number k. The vertical axis response was not corrected for changes in the collection solid angle for the critical modes as a function of rotation. The range of accessible wave numbers is from about 100 rad/cm up to 4×10^4 rad/cm. These limits were discussed in the previous section. Similar k-distribution results were obtained for the 6-μm film. The more complicated angle distributions for the 2-μm film precluded k-distribution measurements in this case.

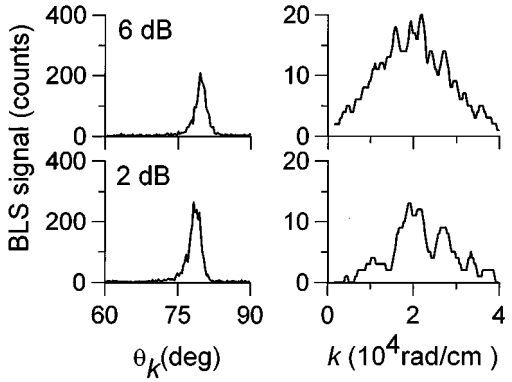

FIG. 6. Representative data on the BLS signal intensity as a function of the diaphragm rotation angle with respect to the direction of the in-plane static magnetic field H. The left-hand-side diagrams are for rotation with the diaphragm axis along the optical axis and the horizontal scales give the in-plane propagation angle θ_k. The right-hand-side diagrams are for rotation with the diaphragm shifted off axis and the horizontal scales give values of the wave number k, the converted magnitude of the in-plane component of the selected spin-wave wave vector. These data are for the 4.15-μm-thick film with H at 1070 Oe. The pump frequency was 9.5 GHz. Power levels for the bottom and top pairs of diagrams were 2 and 6 dB above threshold, respectively. As in Figs. 1 and 2, only the portion of the BLS signal corresponding to magnons at one-half the pump frequency was monitored.

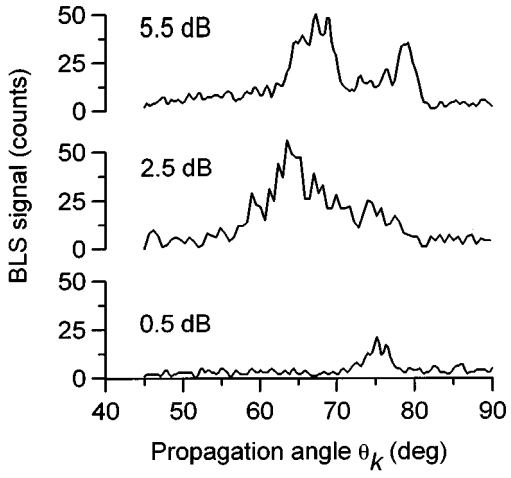

FIG. 7. Data on the BLS signal intensity as a function of the in-plane propagation angle θ_k for the 2-μm-thick film with H at 1068 Oe. Results are shown for three different power levels of 0.5, 2.5, and 5.5 dB above threshold. The pump frequency was 9.5 GHz. As in Fig. 1, only the portion of the BLS signal corresponding to magnons at one-half the pump frequency was monitored.

The wave-number distributions shown in Fig. 6 have many of the same basic features observed for subsidiary absorption in thin films.[4] These distributions are broad and exhibit considerable structure. Although the k distribution does change somewhat with power, the basic features are preserved. It is important to note that the θ_k and k distributions shown in Fig. 6 do not necessarily represent all the critical modes which may be excited in the nonlinear processes. The BLS technique in the forward-scattering configuration can only detect wave numbers up to about 4×10^4 rad/cm, a limit imposed by the size of the collection lens and the scattering geometry. As a result, the distributions in Fig. 6 represent only the low-wave-number part of the critical-spin-wave-mode spectrum that is accessible in the forward-scattering experiment. Nevertheless, even this limited wave-vector distribution regime gives important information about the nonlinear process and the character and behavior of the excited modes.

Both the broad wave-number distributions and the fine structure shown in the right-hand-side diagrams of Fig. 6 are consistent with the previously published results for subsidiary absorption. It is clear that for the particular 4.15-μm-thick film the wave-number distribution is broad with all modes propagating along one θ_k direction. It is noteworthy that the critical-mode wave numbers detected by the BLS experiment are all well within the experimental observation window. This means that the excited critical modes represent the complete low-wave-number $100-4\times10^4$ rad/cm part of the spectrum. As already indicated, additional critical modes with wave numbers out of the experimental window could be, in principle, also present.

The above data show the essential features of the critical-mode behavior at and above the threshold, for in-plane parallel-pumped YIG films. One of the very intriguing features of the overall data is the effect of film thickness on the observed response. Recall, for example, the Fig. 5 result on the broadening in the propagation-angle distribution to the 4.15-μm film at high powers. This broadening with power did not occur for the thickest film, even though the actual threshold microwave fields for the two films were the same for the range of static fields below 1150 Oe. The 2-μm film, on the other hand, did not yield well-defined values of θ_k at high-power levels. Typical results in this case will be considered shortly. Recall also that the threshold versus field results in Fig. 2 did show an increase in threshold for the 2-μm film relative to the other two samples for static fields above 1150 Oe or so. Further measurements were made to study these effects.

Figure 7 shows the results of measurements of the BLS intensity versus the in-plane propagation angle θ_k for the 2-μm film, a static magnetic field of 1068 Oe, and power levels 0.5, 2.5, and 5.5 dB above threshold. These results may be compared with the left-hand-side diagrams in Fig. 6 for the 4.15-μm film at approximately the same static field. At the lowest power, the data show one relatively narrow peak positioned slightly above $\theta_k=75°$. This result is similar to the data in the lower left diagram of Fig. 6. The situation changes significantly at higher powers. At 2.5 dB, the critical mode propagation-angle distribution has broadened and shifted. There appears to be a small residual peak near 75°, but the dominant peak in the distribution has shifted below 65°. The distribution also has evolved to exhibit considerable structure. At 5.5 dB, the distribution has evolved even further. At this power level, there appears to be two well-resolved peaks, one slightly above the low-power 75° position and one in the 65°–70° range. This appears to be direct observation of the splitting of a parametrically excited spin wave above threshold. This point will be considered further in the next section. Recall that the critical-mode angular distribution in Fig. 6 for the 4.15-μm sample does not change at all as the power is increased to 6 dB above threshold. In that

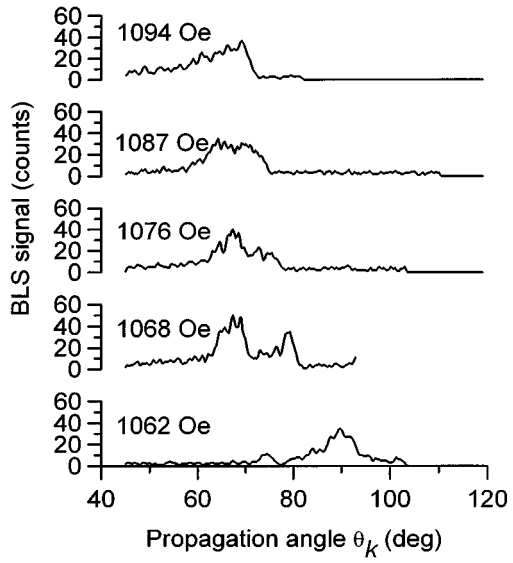

FIG. 8. Data on the BLS signal intensity as a function of the in-plane propagation angle θ_k for the 2-μm-thick film. The incident power was 5.5 dB above threshold in all cases. The value of the static magnetic field H was varied from 1062 to 1094 Oe, as indicated. The pump frequency was 9.5 GHz. As in Fig. 1, only the portion of the BLS signal corresponding to magnons at one-half the pump frequency was monitored.

case, as well as for the 6-μm film, the angular distribution remains narrow and well focused over the entire range of accessible powers.

BLS intensity versus in-plane propagation angle θ_k for the 2-μm film was also measured for different values of the static magnetic field from 1062 to 1094 Oe, all at a relatively high-power level of 5.5 dB above threshold. These results are shown in Fig. 8. The field values are indicated in each of the five diagrams. Note that these fields correspond to the bottom region of the butterfly curve in Fig. 2. Recall that in this regime, the thresholds were essentially the same for the three films. Recall also that the two thicker films had narrow propagation-angle distributions and well-defined values of θ_k.

As the Fig. 8 data show, the situation is quite different for the 2-μm film. The angle distribution at the lowest field value of 1062 Oe, essentially at the butterfly-curve minimum, has a main peak close to 90°. This peak corresponds to the expected critical mode θ_k value from the bulk theory at this field, as indicated in Fig. 4. However, the lower diagram in Fig. 8 also shows a small but distinct peak close to a rotation angle of 75°. This double-peak effect becomes even more pronounced as the static field is slightly increased to 1068 Oe. The 1068-Oe trace in Fig. 8 is the same as the upper trace in Fig. 7. Note that the peaks are shifted down, as expected, for critical modes at one-half the pump frequency and fields above the butterfly-curve minimum. As the field is further increased, the two distinct peaks merge to yield a broad angular distribution with considerable structure. For the two highest field traces shown, this broad distribution is shifting down in angle as the field is increased and the shape of the distribution appears to be changing.

This section has described the results on the critical-mode properties for parallel pumping in thin YIG films. The data on propagation-angle and in-plane wave-vector-component distributions for the critical modes as a function of power and static magnetic field for 2-, 4.15-, and 6-μm-thick films yielded a number of new results. First, the propagation-angle distributions were quite different for the 2-μm film, relative to the two thicker films. The thicker films had narrow propagation-angle distributions with well defined values of $\theta_{k\text{-crit}}$ defined as the critical-mode in-plane propagation angle relative to the field direction. These characteristics persisted to high-power levels. The 2-μm film, on the other hand, had well-defined $\theta_{k\text{-crit}}$ values only for powers just above threshold. At higher powers, the distributions became bimodal and evidenced considerable structure and broadening. The high-power distributions also showed a very strong dependence on the static magnetic field. A possible precursor effect in the propagation-angle distributions was found for the 4.15-μm film, in that the width of the distribution increased substantially at high power.

A well-defined θ_k is needed in order to measure critical-mode k distributions. The distributions in the in-plane wave-vector component for the critical modes could only be measured for the 4.15- and 6-μm films. These distributions were broad and showed considerable structure, similar to the results for subsidiary absorption[4] and resonance saturation.[5]

IV. DISCUSSION

While the results presented above have some limited correlations with existing bulk theories, the different results as a function of film thickness and the complicated distributions in in-plane propagation angle and wave-vector component have no basis in these theories. This section will review the essential elements of the bulk theory, make connections where possible between the present data and the bulk analysis, and consider further implications of the experimental results on the critical-mode angle and wave-number distributions.

The bulk theory of parallel pumping was initially done by Schlömann[6,7] and further developed by Patton.[10] The basic formula from the bulk theory for the spin-wave instability threshold microwave field amplitude h_{crit} for parallel pumping is given by

$$h_{\text{crit}} = \min\left\{ \frac{\omega_p}{|\gamma| 4\pi M_s} \frac{\Delta H_k(k)}{\sin^2 \theta_k} \right\}_{\mathbf{k},\omega_k=\omega_p/2} . \qquad (1)$$

In Eq. (1), ω_p is the pump frequency, $|\gamma|$ is the absolute value of gyromagnetic ratio, $4\pi M_s$ is the saturation induction, $\Delta H_k(\mathbf{k})$ is the wave-vector $\mathbf{k}$-dependent spin-wave linewidth, θ_k is the spin-wave propagation angle between the spin-wave wave vector $\mathbf{k}$ and the direction of the vector static magnetic field $\mathbf{H}$, and ω_k denotes the spin-wave frequency. Operationally, one obtains the theoretical h_{crit} for a given static field H by minimizing the expression in curly brackets in Eq. (1) over all possible spin-wave wave-vector $\mathbf{k}$ states available at a spin-wave frequency ω_k equal to one-half the pump frequency. Plots of h_{crit} versus H then correspond to the butterfly curves discussed at length in the literature.[11] The values of k and θ_k which yield the minimum

threshold at a given field, along with the frequency $\omega_k=\omega_p/2$, define the critical-mode wave number $k_{\rm crit}$ and spin-wave angle $\theta_{k\text{-crit}}$.

The shapes of the theoretically obtained butterfly curves and the field-dependent $k_{\rm crit}$ and $\theta_{k\text{-crit}}$ values obtained by this procedure are strongly influenced by both the details of the spin-wave dispersion relation for $\omega_k(\mathbf{k},\mathbf{H})$ and the $\mathbf{k}$ dependence of the spin-wave linewidth. A detailed discussion of the basic effects is given in Ref. 11. The dispersion relation appropriate for YIG may be written as

$$\omega_k=|\gamma|[(H_i+Dk^2)(H_i+Dk^2+4\pi M_s\ \sin^2\theta_k)]^{1/2}. \quad (2)$$

In Eq. (2), H_i is the effective internal static field which includes anisotropy effects and static demagnetizing fields as well as the static applied field, and D denotes an exchange field parameter. The spin-wave linewidth $\Delta H_k(\mathbf{k})$ for the parallel-pumping configuration may be taken in the form[11]

$$\Delta H_k=A_0+A_1\ \sin^2(2\theta_k)+A_2k, \quad (3)$$

where A_0, A_1, and A_2 represent adjustable parameters which may be used to fit particular data.

The solid and dashed lines in Fig. 2 show the best-fit butterfly curves to the data for the two thicker films and the 2-μm-thick film, respectively, based on Eqs. (1)–(3). The fits were obtained with typical values for the YIG materials parameters, namely, $|\gamma|/2\pi=2.8$ GHz/kOe, $4\pi M_s=1750$ Oe, and $D=5.4\times10^{-9}$ Oe cm^2/rad^2. The theoretical position of the butterfly-curve minimum was fitted to the observed minimum threshold at $H=1060$ Oe by adjusting H_i downward by 30 Oe to account for anisotropy shifts. The vertical axis in Fig. 2 shows relative threshold values only. The best fit to the data for the 4.15- and 6-μm-thick films was obtained for values of A_1/A_0 and A_2/A_0 of 0.433 and 3.33×10^{-6} Oe rad/cm, respectively. For the 2-μm film, the fit required a change A_1/A_0 to 0.75.

The fits to the data shown in Fig. 2 and the values of the parameters needed to accomplish these fits are quite reasonable. However, there is no *a priori* reason to use a different A_1/A_0 value for the different films. In the bulk theory, film thickness does not enter into the theory at all. However, one justification of the above fitting procedure with different values of A_1/A_0 for the two fits may be found in the results of Ref. 9 for subsidiary absorption. Here it was found that the *ad hoc* $A_1\sin^2(2\theta_k)$ term in the spin-wave linewidth had its origin, not in spin-wave relaxation, but in the actual quantization of the spin-wave modes for the thin film. If this conclusion is also valid for parallel pumping, one has an immediate operational justification for the use of the A_1/A_0 ratio as an adjustable parameter. Unfortunately, the extension of the analysis of Ref. 9 to parallel pumping is neither straightforward nor simple. A bona fide thin-film theory for parallel pumping would need to take into account the finite sizes of the sample in all directions. Such an analysis has not yet been done.

Now consider the critical mode θ_k data shown in Fig. 4. The solid line in Fig. 4 was obtained with the same parameters listed above. The A_1/A_0 ratio had a negligible effect on this curve. The curved portion of the solid line above $H=1060$ Oe comes essentially from Eq. (2) with the spin-wave frequency ω_k set to $\omega_p/2$ and the wave number k set to zero. The agreement between the solid line and data is reasonable, especially if one considers the fact that no special effort was made to find an optimum combination of YIG parameters to achieve a best fit to these θ_k data. The more rapid falloff in θ_k with increasing field which is observed experimentally is one more indication of the need for a bona fide thin-film parallel pumping theory.

The above results apply to the critical-mode situation at threshold. At present, there is no basis in theory upon which to address the experimental results for power levels above threshold. It is noteworthy, however, that a critical-mode splitting well above the instability threshold for parallel pumping was predicted in the mid-1970s by Zakharov *et al.*[12] The specific prediction from Ref. 12 was for a YIG sphere, with a splitting of the critical mode into two different modes at a microwave-field amplitude of $1.87h_{\rm crit}$ or, equivalently, at a power about 5.5 dB above the threshold. This prediction appears to be in agreement with the present experimental results. Such agreement should be approached with caution, however. Several issues need clarification. (i) A clear connection needs to be made between the theory and experiment for the thin-film geometry. The theory in Ref. 12 was for sphere-shaped samples only. (ii) The critical-mode splitting found experimentally is confined to the thinnest film only. No splitting at all was found for the two thicker films. Any complete theoretical model must take this difference into account. (iii) The theory of Ref. 12 predicts the onset of the critical-mode splitting as a threshold effect, with a second critical power level similar to the first threshold level for the onset of the spin-wave instability. The experimental results in Figs. 6 and 7 show a more gradual transition from a single well-defined $\theta_{k\text{-crit}}$ to critical-mode splitting. The transition is accompanied, moreover, by substantial broadening and fine-structure development. It is clear that the critical-mode evolution as a function of power above the threshold is complex.

The data for the 4.15-μm-thick film in Fig. 6 show a broad k distribution with considerable fine structure, even at power levels close to the threshold. Recall that the number of excited modes at the threshold is not large enough to allow for the measurement of these distributions exactly at the instability threshold. It is reasonable to assume though that only a few modes are initially excited just at $h_{\rm crit}$ and that the distribution of critical modes expands rapidly, as one moves above the threshold by even a small amount. From Fig. 6, it is clear than even at 2 dB above the threshold level, the k distribution is broad and has a well-developed fine structure. It is clear that a large number of modes are participating in the instability process at this power level.

The other significant observation from the k-distribution data follows from the size of these wave numbers. The predictions from the bulk theory for this region of the butterfly curve are for critical modes very close to $k=0$. For samples with lateral dimensions of several mm, $k=0$ would really correspond to in-plane wave-vector-component magnitudes on the order of 10–50 rad/cm. The measured k values are in the 10^4 rad/cm ranges. As discussed at length in Ref. 9, a similar discrepancy between the bulk theory and BLS data is found for subsidiary absorption in thin YIG films. In that case, it was found that a more complete analysis which considered the lateral standing modes across the film yielded

critical-mode predictions as well as complete butterfly curves which were in excellent agreement with the measurements. What is presently needed is a corresponding theory for the parallel-pumping instability threshold in thin films. The prediction of critical modes in the $k=10^4$ rad/cm range will be one crucial test of any such theory.

V. SUMMARY AND CONCLUSION

Several results have been obtained from BLS measurements of the threshold microwave powers and low-wave-vector critical-mode properties for parallel pumping in YIG films. (i) The observed critical-mode wave-number distribution for parallel pumping is broad and has a distinct structure which depends on the static magnetic field and the microwave-power level. This result is similar to that obtained for subsidiary absorption. (ii) The in-plane angle distribution broadens and splits at high-power levels in the case of the 2-μm film, but this was not observed for the 4.15- or 6-μm films. (iii) The bulk parallel-pumping theory correctly predicts the gross features of the butterfly-curve response and critical-mode properties, but cannot explain the observed wave-number dependence or critical-mode propagation direction behavior above the threshold. (iv) The data indicate the need for a refined parallel-pumping theory which would include the effect of the thickness and the lateral dimensions of the sample.

ACKNOWLEDGMENTS

Dr. G. W. was supported in part by the Deutsche Forschungsgemeinschaft, Bonn, Germany. The YIG films used in this work were kindly provided by Dr. J. D. Adam, Northrop Grumman Science and Technology Center, Pittsburgh, PA. The research was supported in part by the U.S. Office of Naval Research, Grant Nos. N00014-91-J-1324 and N00014-94-1-0096, the National Science Foundation, Grant Nos. DMR-8921761 and DMR-9400276, and the U.S. Army Research Office, Grant No. DAAL03-91-G-0327.

*On leave from the Faculty of Electrical Engineering and Information Technology of the Slovak Institute of Technology, Bratislava, Slovakia.

†Present address: ABB Hochspanungstechnik AG, Zurich, Switzerland.

‡Present address: Bosch Telecom GmbH, Frankfurt, Germany.

[1] W. Wettling, W. D. Wilber, P. Kabos, and C. E. Patton, Phys. Rev. Lett. **51**, 1680 (1983).

[2] W. D. Wilber, W. Wettling, P. Kabos, C. E. Patton, and W. Jantz, J. Appl. Phys. **55**, 2533 (1984).

[3] W. D. Wilber, J. G. Booth, C. E. Patton, G. Srinivasan, and R. W. Cross, J. Appl. Phys. **64**, 5477 (1988).

[4] P. Kabos, G. Wiese, and C. E. Patton, Phys. Rev. Lett. **72**, 2093 (1994).

[5] P. Kabos, C. E. Patton, G. Wiese, A. D. Sullins, E. S. Wright, and L. Chen, J. Appl. Phys. **80**, 3962 (1996).

[6] E. Schlömann (unpublished).

[7] E. Schlömann, J. J. Green, and U. Milano, J. Appl. Phys. **31**, 386S (1960).

[8] Interferometer system manufactured by JRS Ltd., Zwillikerstrasse 8, 8910 Affoltern a A., Switzerland.

[9] G. Wiese, P. Kabos, and C. E. Patton, Phys. Rev. B **51**, 15 085 (1995).

[10] C. E. Patton, Phys. Status Solidi B **92**, 211 (1979).

[11] See, for example, M. Chen and C. E. Patton, in *Nonlinear Phenomena and Chaos in Magnetic Materials*, edited by P. E. Wigen (World Scientific, Singapore, 1994), pp. 33–82.

[12] V. E. Zakharov, V. S. L'vov, and A. S. Starobinets, Usp. Fiz. Nauk **114**, 609 (1974) [Sov. Phys. Usp. **17**, 896 (1975)].